Dynamic screening and plasmon spectrum in bilayer graphene

Wen-Long You and Xue-Feng Wang*
School of Physical Science and Technology, Soochow University, Suzhou, Jiangsu 215006, People's Republic of China

We have theoretically studied the collective response properties of the two-dimensional chiral electron gas in bilayer graphene within the random phase approximation. The cooperation of external controlling factors like perpendicular electric bias, temperature, doping, and substrate background provides great freedom to manipulate the dynamic dielectric function and the low-energy plasmon dispersion of the system. Intriguing situations with potential application are systematically explored and discussed. Extra undamped plasmon modes might emerge under electric bias. They have almost zero group velocities and are easy to manipulate.

PACS numbers: 71.10.-w,75.10.Lp,75.70.Ak,71.70.Gm

I. INTRODUCTION

Experimental breakthrough in isolation of high-quality few-layer graphene by exfoliation and epitaxial growth has led to intense experimental and theoretical interest in graphene materials [1]. Recently, much interest has been focused on the AB-Bernal stacked bilayer graphene (BLG) for fundamental physics and application potential in nanotechnology [2–23]. With its own special nature, BLG inherits some characteristics of the monolayer graphene (MLG) carrying chiral Dirac fermions. Intrinsic BLG is identified as a zero-gap semiconductor with quadratic band dispersion in low-energy regime instead of the linear band dispersion in MLG. In such a case, the density of state (DOS) in BLG at the two nonequivalent Dirac points, called the K and K' points, is a constant, in contract to vanishing DOS in MLG. Hence, BLG shares some similar features with two-dimensional electron gas (2DEG). Specifically, an energy gap between the conduction and valence bands can be easily opened and tuned by introducing an electrostatic potential bias between the two graphene layers [2–6]. The bias modifies the parabolic band structure, and increases the DOS at the top of the valance band and the bottom of conduction band.

Previous studies have clearly evidenced that Coulomb interactions play a significant role in graphene [24, 25]. Similarly, electron-electron interactions in BLG can also lead to exotic phenomena. The many-body effects are crucial to understanding the transport and optical properties of the system. A particularly fruitful phenomenon is the dynamic screening. The frequency dependent screening determines the elementary quasiparticle spectra as well as the collective modes. At zero temperature, the screening properties and the plasmon spectrum in BLG have been studied analytically in the two- and four-band approximations [7–10]. For systems at finite temperature and under electric bias, numerical calculations have been employed to study the properties in the two-band approximation [11, 12]. Because of the distinguished energy band dispersions and chiralities, Coulomb screening properties and collective excitations in BLG exhibit significantly different behavior from the MLG and conventional 2DEGs. Experimentally the plasmon spectra and damping properties in graphene structures have been studied by methods such as electron-energy-loss spectroscopy (EELS) [26–29].

Surface plasmon modes have been used for the rapidly developing terahertz (THz) technology [30, 31] and stimulated emission of plasmon in graphene has been proposed to be used as THz laser at room temperature [32]. One efficient way to increase the net plasmon gain is to decrease the group velocity of plasmon in the system. The plasmon dispersion in BLG is similar to that in MLG and might be easier to manipulate with the help of applied electric bias between the two layers. In this paper, based on Ref.[12], we numerically study the dynamic screening properties of the Coulomb interaction in BLG systems within the random phase approximation (RPA) and consider a fair general situation in which both the temperature and the bias voltage are finite. We calculate the dielectric function of BLG $\epsilon(\mathbf{q},\omega)$ at arbitrary wavevectors $\mathbf{q}$ and frequency ω. The zeros of the real part ϵ_r give the dispersion of the plasmon modes; the imaginary part ϵ_i indicates their damping properties to single particle excitations; the imaginary part of $1/\epsilon$ is related to their optical spectral weight. Beyond from Ref.[12], here we have explored systematically and in a high accuracy the screening properties and the plasmon spectra in a wide parameter space, and in some parameter regimes have found two extra plasmon modes with almost zero group velocities.

II. MODEL

Since there are four inequivalent carbon atoms, the BLG system should be described by the four-band model which gives a hyperbolic dispersion [18]. In the four-band model, a split-off band is located at $\Delta \approx 0.4$ eV above the lowest conduction band and a sombrero shape of band is

*Electronic address: xf˙wang1969@yahoo.com

formed at the bottom of the conduction band in the existence of electric bias. If the Fermi energy (≈ 45.4 meV under $U = 60$ meV for $n = 10^{12}$ cm^{-2}) plus the thermal energy (≈ 26 meV at $T = 300$ K) is much lower than Δ, the effect from the split-off band should be negligible. For a bias potential $U = 60$ meV, the height of the sombrero is $\delta U = 0.5U(1-\Delta/\sqrt{U^2+\Delta^2}) \approx 0.3$ meV [4, 18]. In systems with carrier density n higher than the critical density $n_c = U^2/(\pi\hbar^2 v_F^2)$ (0.27×10^{12} cm^{-2} for $U = 60$ meV), the Fermi energy is above the sombrero and the topology of the Fermi surface is not affected by the sombrero. In this case, the effect of the sombrero appears as a DOS broadening (with a width of the height of the sombrero) at the bottom of the conduction band. Since one part of the thermal effect is also similar to a DOS broadening with a width of the thermal energy, the effect of the sombrero can also be neglected if the thermal energy is much higher than the sombrero height. Therefore, the low-energy properties of the system can be qualitatively well characterized by the two-band parabolic approximation which is valid in the range of density n (0.5 to 2 $\times 10^{12}$ cm^{-2}), temperature T (4.2 to 300 K), and bias potential U (up to 60 meV) most interested in this study. Within such a picture, a pair of chiral parabolic electron and hole bands touch each other at the Dirac (or the charge neutrality) point, and each band has a four-fold degeneracy arising from spin and valley degrees of freedom. Note that the quadratic band dispersion in the two-band approximation deviates from the hyperbolic band dispersion predicted by the four-band model even in the intermediate energy regime. The corresponding results in some situations might differ quantitatively from those in real systems. For the sake of completeness, some zero-temperature results of systems with low carrier density, where the sombrero effect might not be negligible, are presented in the following.

The low-energy effective Hamiltonian describing electrons of moderate energies in the K valley of biased BLG reads as [18]

$$H_K = \frac{\hbar^2}{2m^*}\begin{pmatrix} 0 & k_-^2 \\ k_+^2 & 0 \end{pmatrix} + \frac{U}{2}\begin{pmatrix} 1 & 0 \\ 0 & -1 \end{pmatrix} \quad (1)$$

In the first term, the wavevector $\mathbf{k} = (k_x, k_y)$ with $k_\pm = k_x \pm i k_y$ is measured from the K point; the effective mass is $m^* = \gamma/(2v_F^2) \approx 0.035 m_0$ with γ the interlayer tunneling amplitude inherent in the BLG system, v_F the graphene Fermi velocity, and m_0 the free electron mass. The second term arises from the electrostatic potential bias U between the two graphene layers separated by a distance $d = 3.35\mathring{A}$. The eigenenergy and eigenwavefunction of the above Hamiltonian read [12]

$$E_{\mathbf{k}}^{\lambda} = \lambda\sqrt{(\frac{\hbar^2 k^2}{2m^*})^2 + (\frac{U}{2})^2}, \quad (2)$$

$$\Psi_{\mathbf{k}}^{\lambda} = e^{i\mathbf{k}\cdot\mathbf{r}}\begin{pmatrix} \sin(\frac{\alpha_{\mathbf{k}}}{2} + \frac{1+\lambda}{4}\pi) \\ -\cos(\frac{\alpha_{\mathbf{k}}}{2} + \frac{1+\lambda}{4}\pi)e^{i2\theta_{\mathbf{k}}} \end{pmatrix}, \quad (3)$$

where $\lambda = \pm 1$ denotes respectively the conduction and the valence band. Here $\theta_{\mathbf{k}}$ is the azimuth of the vector $\mathbf{k}$, i.e., $\tan\theta_{\mathbf{k}} = k_y/k_x$, $k = |\mathbf{k}|$, and $\alpha_{\mathbf{k}}$ indicates the ratio of the kinetic energy to the potential bias with $\tan\alpha_{\mathbf{k}} = \hbar^2 k^2/(m^* U)$. For such an energy dispersion the DOS of the system is

$$D(E) = \frac{g_\nu}{(2\pi)^2}\int \frac{dS}{|\nabla_{\mathbf{k}} E|} = \frac{m^*}{\pi\hbar^2}\frac{E}{\sqrt{E^2 - (\frac{U}{2})^2}}, \quad (4)$$

where g_ν is a constant degeneracy factor. Here $g_\nu = 4$ comes from the degenerate two spins and two valleys at K and K'. Under finite bias U, the DOS of the BLG diverges on the edge of the energy gap $E = |U/2|$. It has been shown that the static dielectric constant at $\mathbf{q} = 0$ in intrinsic BLG is much larger than that in MLG due to the presence of a finite DOS at the K point [11, 12]. The bias might further modify the system's properties in a large range of variety.

The wavevector and frequency-dependent dielectric function $\epsilon(\mathbf{q}, \omega)$ tells the response of the system to a weak external perturbation, and determines a variety of many-body related terms such as self-energy, carrier lifetime, and mobility, as well as characterization of other excitations. In the RPA, it is given as

$$\epsilon(\mathbf{q}, \omega) = 1 - v_q \Pi(\mathbf{q}, \omega), \quad (5)$$

where $v_q = e^2/(2\varepsilon_0\varepsilon_b q)$ (with the background dielectric constant ε_b) is the Fourier transformation of the bare Coulomb interaction and the electron-hole propagator is originated from the bare bubble diagram [12]

$$\Pi(\mathbf{q}, \omega) = 4\sum_{\lambda,\lambda',\mathbf{k}} |g_{\mathbf{k}}^{\lambda,\lambda'}(\mathbf{q})|^2 \frac{f(E_{\mathbf{k}+\mathbf{q}}^{\lambda'}) - f(E_{\mathbf{k}}^{\lambda})}{\omega + E_{\mathbf{k}+\mathbf{q}}^{\lambda'} - E_{\mathbf{k}}^{\lambda} + i\delta}. \quad (6)$$

Here $f(x)$ is the Fermi function and the vertex factor reads

$$\begin{aligned} |g_{\mathbf{k}}^{\lambda,\lambda'}(\mathbf{q})|^2 &= |\langle \mathbf{k}+\mathbf{q}, \lambda' | e^{i\mathbf{q}\cdot\mathbf{r}} | \mathbf{k}, \lambda\rangle|^2 \\ &= \frac{1}{2}\left[1 + \lambda\lambda'\cos\alpha_{\mathbf{k}}\cos\alpha_{\mathbf{k}+\mathbf{q}}\right. \\ &+ \left.\lambda\lambda'\sin\alpha_{\mathbf{k}}\sin\alpha_{\mathbf{k}+\mathbf{q}}\cos(2\theta_{\mathbf{k}} - 2\theta_{\mathbf{k}+\mathbf{q}})\right] \quad (7) \end{aligned}$$

When $\mathbf{q} = 0$ and $\mathbf{q} = -2\mathbf{k}$, $|g_{\mathbf{k}}^{\lambda,\lambda'}(\mathbf{q})|^2 = \frac{1}{2}(1 + \lambda\lambda')$. Similar to unbiased BLG, the interband vertical and back scatterings are both forbidden but the intraband back scattering is allowed in biased BLG. For intraband scattering with $\mathbf{k} \perp \mathbf{k}+\mathbf{q}$, we have $|g_{\mathbf{k}}^{\lambda,\lambda'}(\mathbf{q})|^2 = \frac{1}{2}[1 + \cos(\alpha_{\mathbf{k}} + \alpha_{\mathbf{k}+\mathbf{q}})]$, which becomes zero in unbiased BLG [12].

III. RESULT AND DISCUSSIONS

The electron-hole propagator is composed of intra- ($\lambda = \lambda'$) and inter-band ($\lambda = -\lambda'$) components. The intraband component is expected to be similar to that in conventional 2DEGs except the effect of chirality and

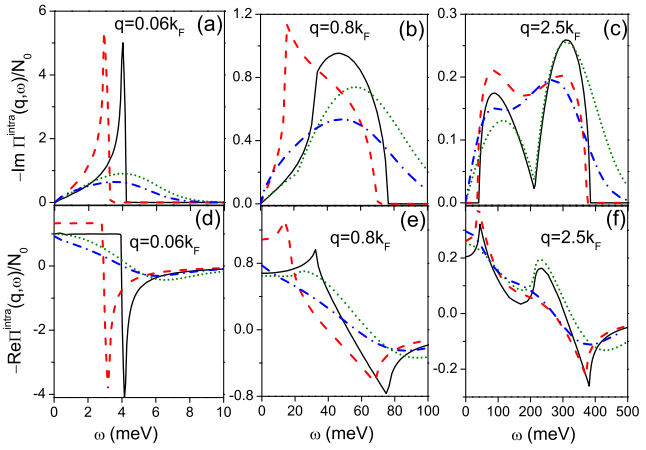

FIG. 1: The negative intraband electron-hole propagator in unit of N_0 versus frequency ω in unbiased/biased BLG at zero/room temperature. The imaginary part for $q = 0.06$, 0.8, and $2.5k_F$ is plotted in panel (a), (b), and (c), respectively, and the corresponding real part in (d), (e), and (f). The electron density is $n = 10^{12}$ cm^{-2} with the Fermi wavevector $k_F = 1.77 \times 10^8$ m^{-1}. The corresponding Fermi energy is $E_F = 34$ meV at $U = 0$ and $E_F = 45.4$ meV at $U = 60$ meV. Solid curves are for $T = 0$, $U = 0$; dashed $T = 0$, $U = 60$ meV; dotted $T = 300$ K, $U = 0$; dash-dotted $T = 300$ K, $U = 60$ meV.

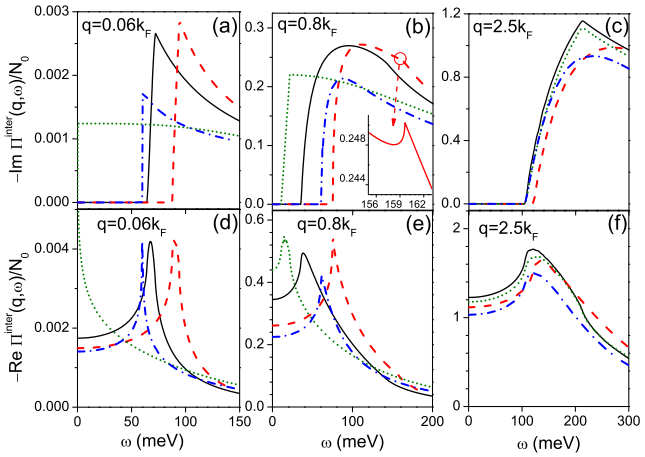

FIG. 2: The negative interband electron-hole propagator in unit of N_0 versus frequency ω is plotted for the same parameters set and arrangement as in Fig.1.

deformation of energy band. The interband one, which can be manipulated by the bias voltage, modifies qualitatively the screening properties of the system. Since the approximate energy spectrum we use in this study is isotropic, the obtained properties are also isotropic and we use $q \equiv |\mathbf{q}|$ and $k \equiv |\mathbf{k}|$ in the following discussion.

In Fig. 1, we plot the negative intraband propagator in unit of $N_0 = 2m^*/\pi$ (the DOS of intrinsic BLG) versus frequency ω for three typical wavevector q values. Similar to the 2DEG result at zero temperature, the imaginary part is nonzero in the single particle continuum $0 < \omega < \omega_u$ for $0 < q < 2k_F$ and $\omega_l < \omega < \omega_u$ for $q > 2k_F$, with $\omega_l = |E^1_{k_F-q} - E^1_{k_F}|$ and $\omega_u = E^1_{k_F+q} - E^1_{k_F}$. The derivative of the imaginary part is not continuous at the continuum edges and for $0 < q < 2k_F$ is also not continuous at $\omega = \omega_l$ besides $\omega = 0$ and ω_u. When the bias U increases, the structures of the curves shift to lower energy because the energy band is narrowed and the group velocity of electrons at the bottom of the conduction band decreases. When the temperature increases, the sharp edges become smoother and the nonzero range gets wider as expected.

Different from the 2DEG result, as illustrated in Fig.1(c) for $q > k_F$ at $U = 0$ and $T = 0$, the imaginary part has a sharp dip with a derivative discontinuity at $\omega_m = q^2/2m^*$ between the edges due to the chiral nature of the wave functions [9]. The dip and discontinuity persist at finite temperature but become softened and disappear under finite bias voltage.

The real part, presented in the lower panels of Fig.1, shows a sharp peak at ω_l and a sharp dip at ω_u with an extra peak near ω_m for $q > k_F$ and moves in a similar way as the imaginary part with bias and temperature. However, the structure near ω_m for both the imaginary and real part develops in a different way from those at ω_l and ω_u when U and T increase. It remains at high temperature and removes off with the bias voltage while those at ω_l and ω_u decay with temperature. On average, the variation range of the propagator decreases with q.

In Fig.2, we present the negative interband propagator in unit of N_0 versus ω for the same three q values as in Fig.1. Its imaginary part and the single particle continuum have a minimal energy limit $\omega_1 = E^1_{k_F} - E^{-1}_{k_F-q}$ at zero temperature or $\omega_2 = 2E^1_{q/2}$ at finite temperature. For small q [Fig.2(a)] the imaginary part increases sharply and reaches a peak before decreases in a way $\sim 1/\omega$. For mediate $q = 0.8k_F$ [Fig.2(b)] the main peak becomes round and smooth while a sharp peak near $\omega_3 = E^1_{k_F} - E^{-1}_{k_F+q}$ appears under bias as shown in the inset of Fig.2(b). This latter peak grows and becomes more visible as U increases. For $q > k_F$ a peak with discontinuity appears near $\omega_m = q^2/2m^*$ at zero temperature in both biased and unbiased BLG [9] as shown in Fig.2(c).

Corresponding to the continuum edges of the imaginary part, on the curve of the real part as shown in the lower panels of Fig.2, there is a peak near ω_1 (ω_2) at low (high) temperature when the electron system is degenerate (nondegenerate). The peak near ω_2 may become very sharp for small q in biased BLG because the bottom (top) of the conduction (valence) band becomes flat and the DOS diverges on the edge of energy gap. The overall contribution of interband excitation to the propagator increases with q and in a way $\sim q^2$ at small q.

As we know, the electron-hole propagator reflects the electric polarizability of a many-body system screening a Coulomb potential. After being reduced by the background dielectric constant ε_b, it determines the dielectric

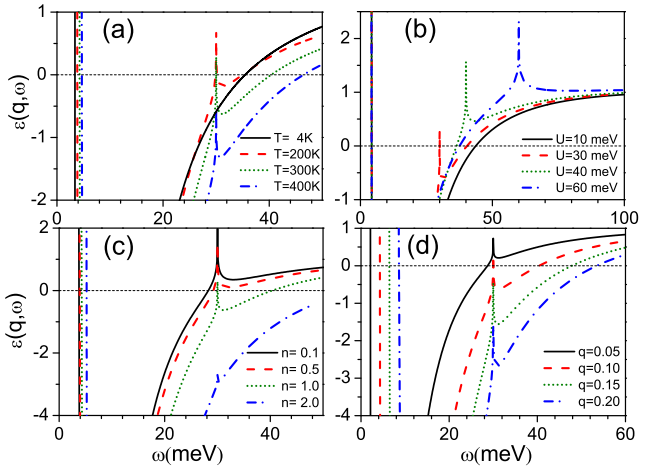

FIG. 3: The real part of the dielectric function ϵ_r vs frequency ω when $\varepsilon_b = 1$ in variety of bias U, temperature T, electron density n ($\times 10^{12}$ m^{-2}), and wavevector q ($\times 10^8$ m^{-1}) is plotted in (a)-(d), respectively. Parameters $U = 30$ meV, $n = 10^{12}$ m^{-2}, $q = 0.1 \times 10^8$ m^{-1}, $T = 300$ K are used if not specified in the panels.

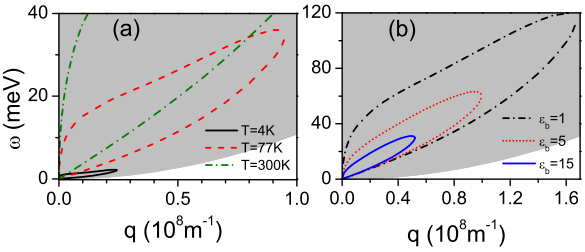

FIG. 4: Plasmon spectrum of intrinsic BLG (a) in vacuum with $\varepsilon_b = 1$ at various temperature and (b) with various dielectric constant at room temperature $T = 300$ K. The shadow shows the electron-hole single-particle continuum at zero temperature.

function $\epsilon(q,\omega) = \epsilon_r + i\epsilon_i$ as indicated in Eq.(5). The zero of the real part ϵ_r gives the collective excitation of the system in the absence of external electromagnetic field. The imaginary part ϵ_i gives the spectrum of the single particle excitation. In the presence of only intraband single particle excitation as in conventional 2DEG, there exist maximally two plasmon modes, one acoustic mode of frequency ω_A within the single particle excitation and another optical mode ω_O, because $-\mathrm{Re}[\Pi(q,\omega)]$ has only one dip below zero as shown in Fig.1. The acoustic mode is thus always overdamped with little spectral weight and not experimentally relevant. The contribution from interband excitation introduces fine structures to ϵ_r near zero and at least two extra modes, ω_3^p and ω_4^p may emerge.

In Fig.3, we display ϵ_r versus ω for various temperature T (a), bias voltage U (b), electron density n (c), and wavevector q (d). In the high frequency limit, the effect of polarization vanishes and $\epsilon_\infty = 1$. For intrinsic BLG where $n = 0$, the intraband polarization is negligible and $\epsilon_r > 0$ at $T = 0$. There is no collective mode. In other cases, the ϵ_r versus ω curve has a deep dip at ω_u and a peak at ω_1 or/and ω_2. The competition in Eq.(5) among value one, the intra-, and inter-band contributions to the polarizability determine its fine features. For typical parameters, as illustrated in Fig.1 and 2, the effect of the intra- (inter-) band polarization decreases (increases) with q so we expect that ϵ_r mainly shows intra- (inter-) band characteristics for long (short) wavelength. In this study we are mostly interested in the screening and collective excitation properties of long wavelength in the system, and in Fig.3 we present the details only for $q \ll k_F$ near $\epsilon_r = 0$.

The result for a system of $U = 30$ meV, $n = 10^{12}$ cm^{-2}, and $q = 0.1 \times 10^8$ m^{-1} is exhibited in Fig.3(a). At low temperature $T = 4$ K (solid) when the system is degenerate, the intraband contribution dominates and a peak appear near $\omega_1 = E^1_{k_F} - E^{-1}_{k_F-q} \simeq 2E^1_{k_F} = 74.4$ meV which is out of the panel. When the temperature increases to 200 K (dashed) and the system becomes non-degenerate, a sharp peak emerge near $\omega_2 = 2E^1_{q/2} \simeq 30$ meV. Since this interband peak is located just below the optical plasmon energy ω_O, it can introduce two extra roots ω_3^p and ω_4^p to the equation $\epsilon_r = 0$, i.e., two extra plasmon modes in the system. The extra plasmon mode of lower energy ω_3^p is out of the interband single particle continuum and can be only weakly damped. When the temperature increases further (dotted and dash-dotted) the enhanced intraband contribution shifts the peak below zero and the extra plasmon modes disappear. In the same time, ω_O increases with the temperature as more electrons (holes) exist in the conduction (valence) band.

As shown in Fig.3(b), the bias voltage can sensitively shift the interband peak and control the emergence of the extra plasmon modes. These modes have energies (frequencies) proportional to the bias voltage and group velocities close to zero. The increase of the electron density enhances the degeneracy of the system and reduces the amplitude of the interband peak at $\omega_2 = 2E^1_{q/2}$ as plotted in Fig.3(c). The enhanced intraband contribution at higher density also increases the frequency of the optical plasmon mode ω_O.

In Fig.3(d) we illustrate how the ϵ_r-ω curve develops with q at room temperature $T = 300$ K. Overall the intra- (inter-) band contribution to ϵ simply decreases (increases) with q as shown previously in Figs.1 and 2, but their effect on the plasmon spectrum is more complicated due to their competition with each other. When q increases, the intraband introduced ϵ_r dip becomes wide which usually results in the increase of the plasmon frequency. The interband peak of ϵ_r is located at the fixed energy $\omega_2 \simeq 30$ meV and its amplitude increases with q. As a result, only when ω_2 is close to ω_O, the interband contribution can affect significantly the plasmon spectrum.

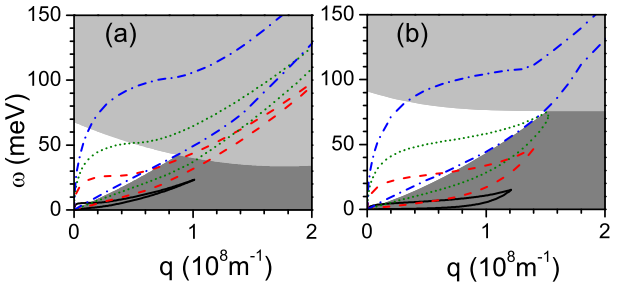

FIG. 5: Plasmon spectrum at zero temperature of (a) unbiased (b) U=60meV biased BLG in vacuum for density $n = 0.1$ (solid), 0.5 (dashed), 1.0 (dotted), and 2.0 (dash-dotted) $\times 10^{12}$ cm^{-2}. The single-particle continuum at $n = 10^{12}$ cm^{-2} is also present (light/dark shadow for the inter-/intra-band part).

The plasmon spectrum in intrinsic BLG (unbiased and undoped) depicted in Fig.4 at various temperatures T (a) and for various background dielectric constant ε_b (b). At zero temperature, there is no carrier and no plasmon mode in the system. At finite temperature, electrons (holes) are excited in the conduction (valence) band and two plasmon modes emerge. In the long-wavelength limit, their frequencies are proportional to $\sqrt{T}$ at high temperature. Similar to the 2DEG result, we also observe a dispersion $\omega_O \propto \sqrt{q}$ and $\omega_A \propto q$. The background dielectric constant can also be employed to modify the plasmon frequency as shown in Fig.4(b). The acoustic mode is not sensitive with ε_b but the frequency of optical mode decreases quickly with ε_b.

In Fig. 5, the plasmon spectrum for various electron densities at zero temperature is illustrated in unbiased BLG (a) and in biased one with $U = 60$ meV (b). In the long-wave limit, $q \sim 0$, the dielectric function is dominated by the intraband contribution. The properties of the system at zero temperature is mainly determined by the group velocity of electrons at the Fermi energy. The plasmon spectrum of unbiased system is similar to that of 2DEG. If the electron density is not high, e.g. $n \lesssim 10^{12}$ cm^{-2} for $U = 60$ meV as shown in Fig.5(b), the Fermi group velocity of electrons decreases when the external electric field is turned on, due to the band deformation, and the plasmon mode becomes softened. With increasing q the interband contribution becomes more important, which reduces the group velocity of the optical plasmon mode. In some cases, the group velocity of plasmon can be close to zero, a favorite situation for the stimulated plasmon emission [32]. For large q, when the optical plasmon branch enters the interband single particle continuum, i.e. $\omega_O > \omega_1$, the effect of interband contribution decreases and the plasmon spectrum has a long tail in unbiased system or when the carrier density is high. However, in biased systems with low carrier density, the effect of the interband contribution can be significant due to the flat band and the plasmon spectrum ends near where the intra- and inter-band single particle continua meet at $\omega_u = \omega_1$.

The competition between the intra- and inter-band contributions may result in two extra plasmon modes for proper U at finite temperature when thermal excitation becomes important as previously discussed in Fig.3. This is an interesting phenomenon because those modes have unique properties and might be used in nanotechnology. In Fig.6, we plot the plasmon spectra of a biased system with $U = 30$ meV at $T = 300$ K and $n = 10^{12}$ cm^{-2} for background dielectric constant $\varepsilon_b = 1$ (solid), 5 (dash-dotted), and 15 (dotted). At room temperature $T = 300$ K, the electronic system is not degenerate and the plasmon spectrum is in general similar to the one of intrinsic BLG as shown in Fig.4(b). However, as shown in Fig.2 and 3, the interband contribution adds a sharp peak at ω_2 which is around U for small q. As a result, the plasmon spectra are deformed at ω_2 and bifurcate in some cases where two extra plasmon modes ω_3^p and ω_4^p emerge as shown in the inset of Fig.6.

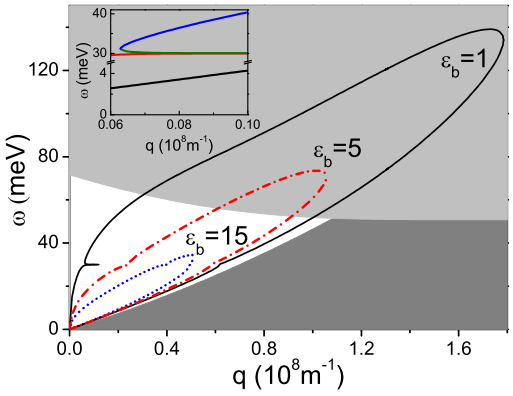

FIG. 6: Plasmon spectrum of biased and doped BLG with $U = 30$ meV and $n = 10^{12}$ cm^{-2} at room temperature $T = 300$ K in environment of different background dielectric constants ε_b. The inset shows the zoomed spectrum of the plasmon branches ω_O,ω_3^p, ω_4^p, and ω_A for $\varepsilon_b = 1$ at small q. The light (dark) shadow shows the interband (intraband) single-particle continuum at zero temperature.

The emerged two plasmon modes have almost zero group velocities and their frequencies are proportional to the bias voltage. In addition, their energies are in the gap of the zero-temperature single particle continuum and the lower one is below the lower limit of single particle excitation, ω_2, at high temperature. This suggests that the modes are undamped or weakly damped and have long lifetime. In Fig.7 we plot the negative imaginary part of the dielectric function, which indicates the spectral weight of the collective modes, for different q. We see that the spectral weigh shows a negligible value (wide peak) near the energy of the acoustic (optical) mode ω_A (ω_O), indicating that the ω_A mode is damped and the ω_O

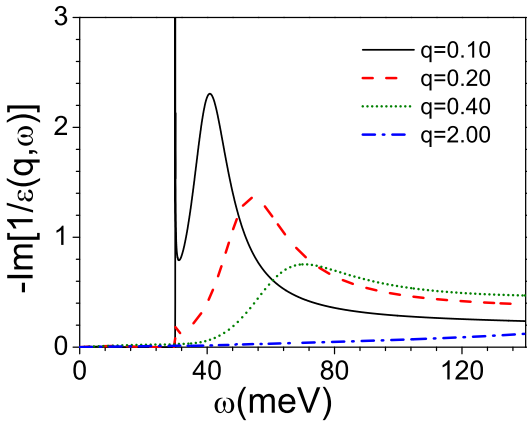

FIG. 7: The spectral weight function versus frequency at various wavevectors q ($\times 10^8$ m^{-1}) for the system with $\varepsilon_b = 1$ in Fig.6.

is weakly damped. In the same time, there is a sharp and high peak at $\omega \backsimeq U$ for small q indicating that the ω_3 and ω_4 modes are almost undamped. These undamped plasmon modes are similar to those in MLG but have lower group velocity. Their energies can be easily manipulated by the bias voltage. These undamped modes with almost zero group velocities then might be used in THz technology [32].

In conclusion, we have studied systematically the many-body response of electrons to external Coulomb perturbation and the plasmon spectra in a biased BLG. The vertical voltage bias opens a gap between the conduction and valence bands and increases the DOSs at the band edges. As a result, the bias modifies the dielectric function greatly. In the long-wave limit, a sharp and controllable dielectric peak might appear at the energy equal to the band gap at high temperature when the system is nondegenerate or at the energy of double the Fermi energy at low temperature when the system is degenerate. In some cases, two extra undamped plasmon modes appear at energies close to the band gap energy and have almost zero group velocities.

Wen-Long You acknowledges the support of the Natural Science Foundation of Jiangsu Province under Grant No. 10KJB140010 and the National Natural Science Foundation (NSFC) of China under Grant No. 11004144. Xue-Feng Wang is supported by NSFC of China (No. 11074182 and 91121021).

[1] T. Ando, J. Phys. Soc. Jpn. **74**, 777 (2005); A. H. Castro Neto, F. Guinea, N. M. R. Peres, K. S. Novoselov, and A. K. Geim, Rev. Mod. Phys. **81**, 109 (2009); D. S. L. Abergel, V. Apalkov, J. Berashevich, K. Ziegler, and T. Chakraborty, Adv. Phys. **59**, 261 (2010); S. Das Sarma, S. Adam, E. H. Hwang, and E. Rossi, Rev. Mod. Phys. **83**, 407 (2011); M.O. Goerbig, Rev. Mod. Phys. **83**, 1193 (2011).
[2] J. B. Oostinga, H. B. Heersche, X. Liu, A. F. Morpurgo, and L. M. K. Vandersypen, Nature Mater. **7**, 151 (2007).
[3] Y. Zhang, T. T. Tang, C. Girit, Z. Hao, M. C. Martin, A. Zettl M. F. Crommie, Y. R. Shen, and F. Wang, Nature (London) **459**, 820 (2009).
[4] E. McCann, Phys. Rev. B **74**, 161403(R) (2006).
[5] H. Min, B. Sahu, S. K. Banerjee, and A. H. MacDonald, Phys. Rev. B **75**, 155115 (2007).
[6] P. Gava, M. Lazzeri, A. M. Saitta, and F. Mauri, Phys. Rev. B **79**, 165431 (2009).
[7] T. Stauber, N. M. R. Peres, F. Guinea, and A. H. Castro Neto, Phys. Rev. B **75**, 115425 (2007).
[8] E. H. Hwang and S. Das Sarma, Phys. Rev. Lett **101**, 156802 (2008).
[9] R. Sensarma, E. H. Hwang and S. Das Sarma, Phys. Rev. B **82**, 195428 (2010).
[10] O. V. Gamayun, Phys. Rev. B **84**, 085112 (2011).
[11] X. F. Wang and T. Chakraborty, Phys. Rev. B **75**, 041404(R) (2007).
[12] X. F. Wang and T. Chakraborty, Phys. Rev. B **81**, 081402(R) (2010).
[13] G. Borghi, M. Polini, R. Asgari, and A. H. MacDonald, Phys. Rev. B **80**, 241402(R) (2009).
[14] G. Borghi, M. Polini, R. Asgari, and A. H. MacDonald, Phys. Rev. B **82**, 155403 (2010).
[15] T. Stauber and G. Gómez-Santos, Phys. Rev. B **85**, 075410 (2012).
[16] R. Nandkishore and L. Levitov, Phys. Rev. Lett. **104**, 156803 (2010).
[17] R. T. Weitz, M. T. Allen, B. E. Feldman, J. Martin, A. Yacoby, Science **330**, 812 (2010).
[18] E. McCann and V. I. Fal'ko, Phys. Rev. Lett. **96**, 086805 (2006).
[19] K. S. Novoselov, E. McCann, S. V. Morozov, V. I. Fal'ko, M. I. Katsnelson, U. Zeitler, D. Jiang, F. Schedin, and A. K. Geim, Nat. Phys. **2**, 177 (2006).
[20] M. I. Katsnelson, K. S. Novoselov, and A. K. Geim, Nat. Phys. **2**, 620 (2006).
[21] A. R. Wright, J. C. Cao, and C. Zhang, Phys. Rev. Lett. **103**, 207401 (2009).
[22] L. Prechtel, L. Song, D. Schuh, P. Ajayan, W. Wegscheider and A. W. Holleitner, Nat. Comm. **3**, 646 (2012).
[23] J. Velasco Jr, L. Jing, W. Bao, Y. Lee, P. Kratz, V. Aji, M. Bockrath, C. N. Lau, C. Varma, R. Stillwell, D. Smirnov, Fan Zhang, J. Jung and A. H. MacDonald, Nat. Nanotech. **7**, 156 (2012).
[24] D. C. Elias, R. V. Gorbachev, A. S. Mayorov, S. V. Morozov, A. A. Zhukov, P. Blake, L. A. Ponomarenko, I. V. Grigorieva, K. S. Novoselov, F. Guinea and A. K. Geim, Nat. Phys. **7**, 701 (2011).
[25] Z. Q. Li, E. A. Henriksen, Z. Jiang, Z. Hao, M. C. Martin, P. Kim, H. L. Stormer and D. N. Basov, Nat. Phys. **4**, 532 (2008).
[26] C. Kramberger, R. Hambach, C. Giorgetti, M. H. Rümmeli, M. Knupfer, J. Fink, B. Büchner, Lucia Reining, E. Einarsson, S. Maruyama, F. Sottile, K. Hannewald, V. Olevano, A. G. Marinopoulos, and T. Pichler, Phys. Rev. Lett. **100**, 196803 (2008).

[27] Y. Liu, R. F. Willis, K. V. Emtsev, and T. Seyller, Phys. Rev. B **78**, 201403(R) (2008).
[28] A. Bostwick, T. Ohta, T. Seyller, K. Horn and E. Rotenberg, Nat. Phys. **3**, 36 (2007); A. Bostwick, T. Ohta, J.L. McChesney, T. Seyller, K. Horn and E. Rotenberg, Eur. Phys. J. Special Topics **148**, 5 (2007).
[29] J. Lu, K. P. Loh, H. Huang, W. Chen, and A. T. S. Wee , Phys. Rev. B **80**, 113410 (2009).
[30] K. L. Wang and D. M. Mittleman, Nature (London) **432**, 376 (2004).
[31] S. A. Maier, S. R. Andrews, L. Martín-Moreno, and F. J. García-Vidal, Phys. Rev. Lett. **97**, 176805 (2006).
[32] F. Rana, IEEE Trans. Nanotech. **7**, 91 (2008).